Mechanisms of Two-Stage Conductivity Relaxation in CdTe:Cl with Ultrasound

Ya. Olikh, M. Tymochko & O. Olikh

Journal of Electronic Materials

ISSN 0361-5235

Journal of Elec Materi
DOI 10.1007/s11664-020-08179-7

Springer

Journal of ELECTRONIC MATERIALS
https://doi.org/10.1007/s11664-020-08179-7

TOPICAL COLLECTION: 19TH INTERNATIONAL CONFERENCE ON II-VI COMPOUNDS

Mechanisms of Two-Stage Conductivity Relaxation in CdTe:Cl with Ultrasound

YA. OLIKH,[1,3] M. TYMOCHKO,[1,4] and O. OLIKH[2]

1.—V.E. Lashkaryov Institute of Semiconductor Physics, NAS of Ukraine, 41, pr. Nauky, Kyiv 03028, Ukraine. 2.—Physics Faculty, Taras Shevchenko National University of Kyiv, Kyiv 01601, Ukraine. 3.—e-mail: jaroluk3@ukr.net. 4.—e-mail: tymochko@ukr.net

We have investigated the kinetics of acoustic relaxation in low-ohmic n-CdTe:Cl crystals in the temperature range 77–200 K when ultrasound (longitudinal waves with a frequency $\sim$ 10 MHz and an intensity $\sim 10^4$ W/m^2) was switched on/off. We found that acoustic conductivity relaxation occurs in two stages. A fast (< 0.6 s) relaxation stage is mainly related to the charge carrier concentration changes and, in part, can be determined by acoustically induced changes of the scattering at dislocations and neutral impurities. A long (> 100 s) stage is mainly caused by the charge carriers mobility changes due to scattering at ionized impurities. We have also discussed possible acoustically stimulated restructuring of point-defective complexes in adjacent crystal regions.

Key words: Ultrasound, CdTe single crystals, point defects, dislocation clusters, Hall effect, scattering mechanisms

INTRODUCTION

The physical properties of real crystals containing structural defects depend not only on the defects concentration but also essentially on the nature of their interaction. In particular, in binary crystals of A_2B_6 and A_3B_5 solid solutions characterized by high dislocation density ($N_{dis} \sim 10^{10}$ m^{-2}), the linear defect interaction with alloying impurities and their complexes can crucially affect the conductivity. The influence of dislocations also increases for films and nanostructures. Of course, uncontrolled electrically active defects degrade properties of semiconductor materials; however, they give possibilities to change the structure of crystal defects by various external fields and to control the physical characteristics of the material. Such data not only give the prospect to control the properties of solids when processing them but also allow one to expect possible changes in their properties during operation. For example, ultrasonic (US) loading of semiconductor crystals or devices can change the defect concentration, their state, and the nature of interdefect interactions, changing the physical properties of the crystals and the working characteristics of devices.[1–3]

CdTe crystals have been used to detect radiation and to construct solar cells.[4,5] However, defects (dislocations, blocks, inclusions, point defect complexes) limit their use. One of the ways to study the interaction of dislocations with other defects is the acoustic Hall method.[1,6,7] As dislocations are the main link to transmit ultrasound energy to electrically active point defects, the acoustical dislocation mechanism is a determinative one. Depending on the sample impurity-defective structure and the ultrasound wave parameters, one can realize both residual and reversible changes observed only under ultrasound action. Dynamic studies give the most information about the mechanisms of the phenomenon. The reason, in particular, is the high lability of the impurity-defective structure of A_2B_6 crystals under ultrasonic loading at low temperatures (< 200 K).[2,8]

(Received November 30, 2019; accepted April 29, 2020)

Published online: 15 May 2020

In earlier works,[8,9] we investigated the ultrasound influence on the electrophysical characteristics of bulk single crystalline CdZnTe samples and studied the relaxation characteristics of the electrical conductivity, $\sigma(t)$, under the ultrasonic load switching on/off. We found acoustically induced (AI) changes in $\sigma(t)$ to be reversible and finishing after the ultrasonic loading. A slow (40–400 s) restoration of the sample parameters occurs. Note that the nature of the AI relaxation of $\sigma(t)$ for different in-dopant chlorine concentration CdTe samples may generally differ.

The paper presents the results of detailed complex electrophysical studies of CdTe:Cl crystals with a pronounced positive effect of AI changes in the electrophysical characteristics at low temperatures.[8] We found that AI relaxation of $\sigma(t)$ occurs in at least two stages showing two ultrasound-driven processes. To discover their mechanisms, we have compared the temperature characteristics of short-term (ST) and long-term (LT) electroconductivity changes in CdTe:Cl samples under US switching on/off, with corresponding temperature changes in the relative contributions of the electron concentration and mobility to the conductivity.

SAMPLES AND METHODS

CdTe:Cl single crystals were grown by the Bridgman vertical method at a low cadmium vapor pressure in the ampoule and then chlorine-doped ($N_{Cl} \approx 10^{24}$ m^{-3}).[10] The x-ray topography method (Williamson–Hall construction) estimated the helical dislocations density, $N_{dis}^{XR} \approx 4 \times 10^9$ m^{-2}.[9] We formed ohmic contacts for the samples by the method of thermal vacuum pollination of indium at 164°C. We measured the concentration $n(T)$ and the mobility $\mu_H(T)$ of the current carriers in the temperature range of 77–300 K by the Hall method in the mode of constant electric and magnetic fields. The magnetic field and propagation of the longitudinal US wave were parallel to the direction [110] (see inset in Fig. 1). The selected non-piezoactive direction of the acoustic wave propagation eliminates the action of the local piezo field.[11] Note also that the US intensity, W_{US} of up to 10^4 W/m^2, used here does not cause deformations exceeding the dynamic material yield point. Therefore, AI dislocation propagation does not occur, as the completely reversible nature of the ultrasound loading influence on the electrophysical (EP) characteristics of the samples shows.

When investigating the EP parameters under ultrasound loading, we used a nitrogen cryostat equipped with acoustic elements. We have described the measurement technique in detail in Refs. [1,6–9] The measurement accuracy of the electric signals under ultrasound loading was up to 2% and that of the temperature about 0.1 K. The accuracy of the Hall coefficient, R_H, and the conductivity, σ, calculation was 3–5%. The sample temperature variation

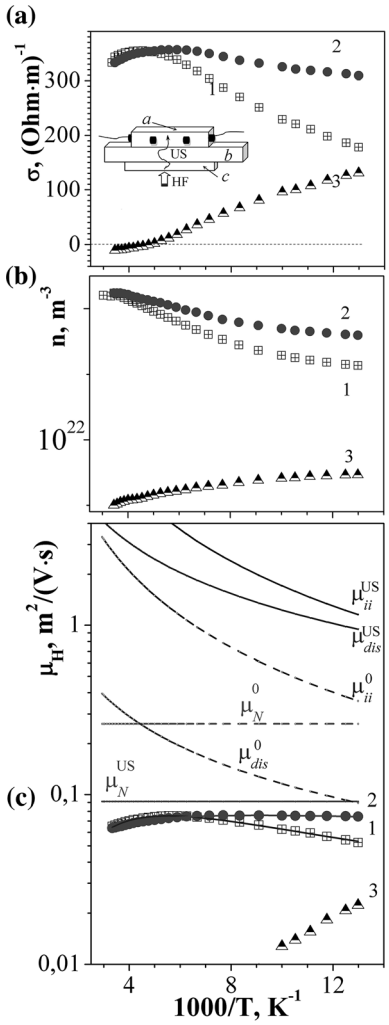

Fig. 1. Temperature dependences of (a) conductivity, (b) electron concentration, and (c) Hall mobility with calculated mobility components for scattering at dislocations μ_{dis}, neutral impurities μ_N and ionized ones μ_{ii}; under ultrasound US and without it 0. In all the figures, curve 1 corresponds to the initial samples, curve 2 to ultrasonic loading $W_{US} \approx 10^4$ W/m^2, and curve 3 to the temperature dependences of the acoustically induced change. The inset in (a) shows the scheme of the acoustic cell: (a) the sample, (b) the buffer, (c) the piezoelectric transducer, HF high frequency, US longitudinal ultrasonic wave.

under intensive US loading in the course of the measurement of a separate experimental point did not exceed ~ 2 K.

We investigated the $\sigma(t)$ relaxation dependences in the same cryostat under the US load switching on/off using a digital multimeter and a related PC. We performed a dynamic study of $\sigma(t)$ with ~ 0.6-s steps. Note that, at such fairly lengthy (5–10 min) measurements in separate $\sigma(t)$ time dependence measurements, the temperature fluctuations, δT, due to ultrasonic heating ranged from 0.1 K to 4 K. We fixed δT for each relaxation dependence and take it into account in the quantitative calculations of $\sigma(t)$.

RESULTS

Ultrasound Influence on Electrophysical Characteristics

Figure 1a shows the electrical conductivity, $\sigma(T)$, temperature dependences for both the original sample and the ultrasonically loaded sample. For low temperatures ($T < 200$ K), we observed AI changes in the $\sigma_i(T)$ dependence. To make the mechanisms of change in $\sigma_i(T)$ under ultrasound loading clear, it is important to separate the AI changes in carrier concentration and mobility, which was done by measuring the Hall effect. We calculated $n_e = (eR_H)^{-1}$ and $\mu_H = R_H\sigma$ in the standard way, and Fig. 1b and c shows their temperature dependences. Under ultrasonic loading (Fig. 1b, curve 2), the electron concentration increases. At room temperature, it is non-essential; however, at nitrogen temperatures, the AI changes reach about 20%. Note that $n(T)$ is monotonous in the whole temperature range, both in the original sample and the ultrasonically loaded sample, being in general slightly dependent on temperature. Figure 1c shows the temperature dependences of separate scattering components obtained by nonlinear approximation of the experimental dependences $\mu_{exp}(T)$ within the differential evolution method.[12]

Relaxation of Conductivity when the Ultrasound is Switched On/Off

AI $\sigma(t)$ changes are completely reversible, and even long (an hour and more) ultrasonic loading does not cause residual changes in the crystal parameters. We found that AI relaxation comes about in two stages (Fig. 2a and b). When switching on/off, we see a short (time < 0.6 s) conductivity, $\Delta\sigma^s_{US}$ ($\Delta\sigma^s_0$), change, after which there is a long-term monotonic relaxation, $\Delta\sigma^l_{US}$ ($\Delta\sigma^l_0$). Therefore, the conductivity change has two components, ST and LT, in the selected notations (see Fig. 2a and b), $\sigma_{US} = \sigma_0 + \Delta\sigma^s_{US} + \Delta\sigma^l_{US}$ and $\sigma_0 = \sigma_{US} - \Delta\sigma^s_0 - \Delta\sigma^l_0$. Here, σ_0 and σ_{US} are the initial (before turning on the ultrasound) and stationary at ultrasonic loading $\sigma(t)$ values, respectively. The first stage, τ_s, goes at < 0.6 s; we have not investigated the kinetics of this stage in more detail. The time of the second stage, τ_l, is 40–400 s which increases with decreasing sample temperature.

Note that, as shown in Fig. 2a and b, $\Delta\sigma^s_0 \neq \Delta\sigma^s_{US}$, $\Delta\sigma^l_0 \neq \Delta\sigma^l_{US}$; however, for the ideal experiment, the above equations must hold. In our opinion, the reason is some methodological disadvantages inherent in our experimental set-up. In particular, the temperature fluctuations, δT, due to ultrasonic heating have ranged from 0.1 K to 4 K in separate $\sigma(t)$ time-dependence measurements; moreover, due to the various durations of relaxation, $\sigma(t)$, measurements when the US is switched on and off, it can also be accompanied by various temperature variations.

Temperature Dependences of ST and LT Conductivity Change Relaxation Components

Figure 3 shows the temperature dependences of the increase/decrease in the absolute value of the short-term ($\Delta\sigma^s_{US}$ and $\Delta\sigma^s_0$) and long-term ($\Delta\sigma^l_{US}$ and $\Delta\sigma^l_0$) components of the AI sample conduction change. One can see in Fig. 3 that the rate of

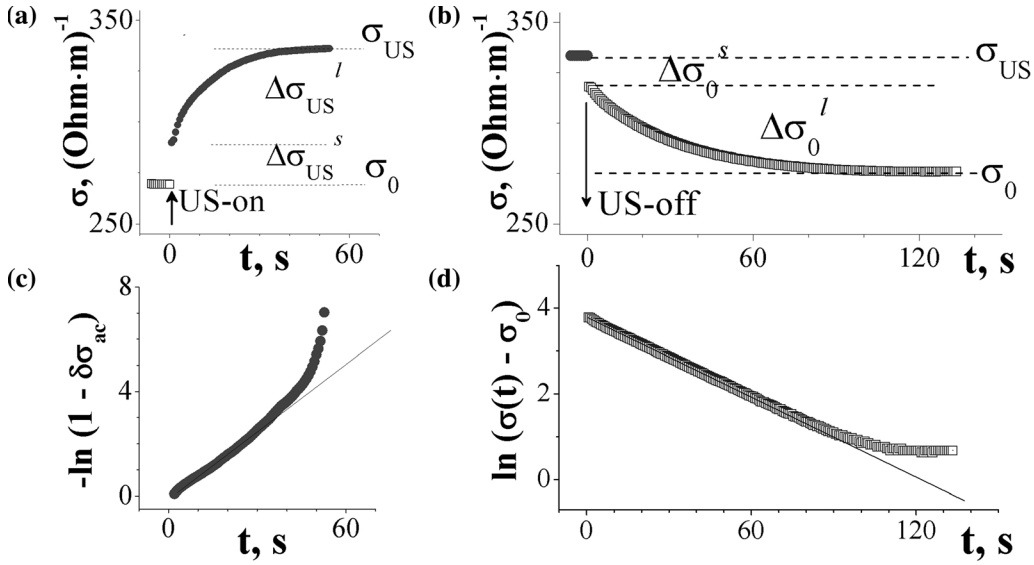

Fig. 2. Typical oscillograms for $\sigma(T)$ at $T \approx 121$ K, where the selected benchmark time milestones are marked for σ_i: (a) when the ultrasonic load is switched on, $\sigma_{US} = \sigma_0 + \Delta\sigma^s_{US} + \Delta\sigma^l_{US}$; (b) when US is switched off, $\sigma_0 = \sigma_{US} - \Delta\sigma^s_0 - \Delta\sigma^l_0$; (c) LT increase curve recovery from oscillogram US-on in the scale $[-\ln(1 - (\sigma - \sigma_0)/(\sigma_{US} - \sigma_0)] = (t/t_{on})$; (d) decrease curve recovery from oscillogram US-off (b) in the scale $\ln(\sigma - \sigma_0) = (-t/t_{off})$. Solid lines in (c) and (d) are linear approximations.

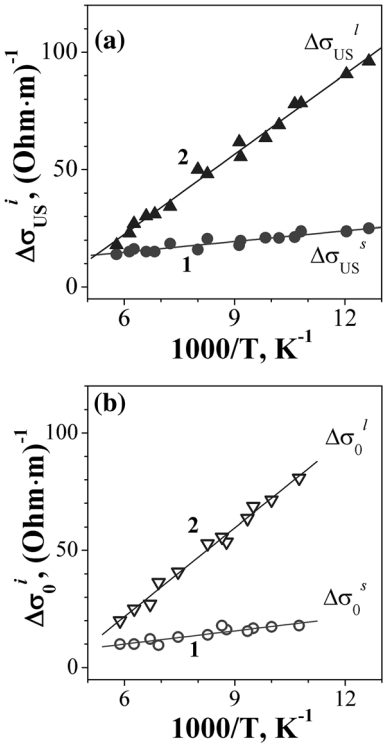

Fig. 3. Experimental temperature dependences for absolute magnitude growth/decrease of ST ($\Delta\sigma_{US}^{s}$ and $\Delta\sigma_0^{s}$, curve 1) and LT ($\Delta\sigma_{US}^{l}$ and $\Delta\sigma_0^{l}$, curve 2) components of Al conductivity changes when ultrasound is (a) switched on and (b) switched off.

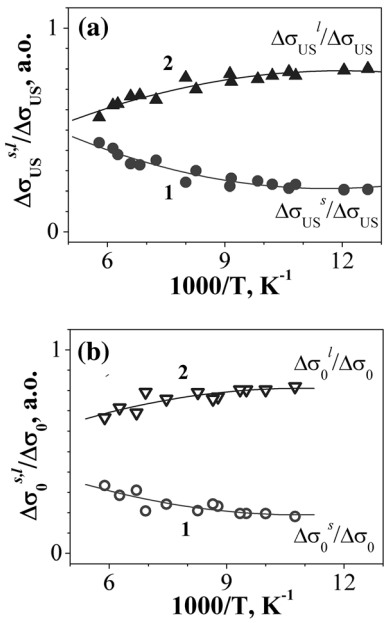

Fig. 4. Experimental temperature dependences for growth/decrease of Al component relative values for instantaneous ($\Delta\sigma_{US}^{s}/\Delta\sigma_{US}$ and $\Delta\sigma_0^{s}/\Delta\sigma_0$, curve 1) and LT ($\Delta\sigma_{US}^{l}/\Delta\sigma_{US}$ and $\Delta\sigma_0^{l}/\Delta\sigma_0$, curve 2) changes of sample conductivity when ultrasound is (a) switched on and (b) switched off.

temperature changes for the long-term components of the increase/decrease in conductivity is much higher (about 6 times) than those for the ST ones, which confirms the qualitative difference between ultrasound action at instantaneous and LT relaxation stages. In particular, the weak temperature dependence for $\Delta\sigma_{US}^{s}$ and $\Delta\sigma_0^{s}$ shows the athermic nature of the process.

Figure 4 shows the ST and LT contributions in the total change of $\sigma(t)$, in which one can see that the temperature dependencies of ST and LT fraction opposing.

Temperature Dependences of Electron Concentration and Mobility Contributions

As the concentration of carriers and their mobility control CdTe conductivity, $\sigma(T) = e{\cdot}n(T){\cdot}\mu(T)$ changes, we can assume that ST and LT $\sigma(t)$ depend on the change of one of just one these parameters. To verify the assumption, we took the experimental data on $n_e(T)$ and $\mu_I(T)$ (Fig. 1b and c, curves 1 and 2) and calculated the temperature dependences of the relative changes in the carrier concentration and their mobility: $\delta n = (n_{US} - n_0)/n_0$, $\delta\mu = (\mu_{US} - \mu_0)/\mu_0$, $\delta\sigma = (\Delta\sigma_{US} - \sigma_0)/\sigma_0$. Then, we calculated their relative contributions to $\sigma(T)$ by the following relationships: $\Delta_\sigma^n(T) = \delta n/\delta\sigma$ and $\Delta_\sigma^\mu(T) = \delta\mu/\delta\sigma$.

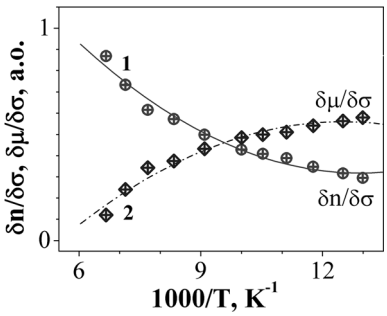

Fig. 5. Temperature dependences of electron concentration $\delta n = (n_{US} - n_0)/n_0$ (curve 1) and mobility $\delta\mu = (\mu_{US} - \mu_0)/\mu_0$ (curve 2) relative parts in the total Al conductivity change $\delta\sigma = (\sigma_{US} - \sigma_0)/\sigma_0$, obtained in Hall measurements.

These dependences of $\Delta_\sigma^n(T)$ and $\Delta_\sigma^\mu(T)$ are shown in Fig. 5. When the temperature decreases, $\Delta_\sigma^n(T)$ weakens, but $\Delta_\sigma^\mu(T)$ increases.

DISCUSSION

Comparison of Temperature Characteristics of Al Changes in Conductivity Relaxation Time Components and Temperature Dependences of Concentration and Mobility Contributions to the Conductivity

Comparison of Figs. 4a and b and 5 shows the corresponding temperature dependences curve correlations: curve 1 in Fig. 4a and b with curve 1 in Fig. 5 and curve 2 in Fig. 4a and b with curve 2 in Fig. 5. This enables us to conclude that the process that prompts an instantaneous relaxation of $\sigma(T)$

when the ultrasound is turned on/off is determined mainly by the acoustic concentration effects; at the same time, AI long-term relaxation processes for $\sigma(t)$ are mainly related to AI changes in mobility.

Comparison of the Acoustic Conductivity Kinetics LT Stage with Photoconductivity

Figure 2a and b illustrates the similarity between the acoustic conductivity (AC) LT phase and the kinetics of photoconductivity (PC) in high-resistance inhomogeneous CdTe semiconductor crystals.[13,14] We use this formal similarity to reconstruct the LT $\sigma(t)$ relaxation curves in Fig. 2a and b, according to the scheme used to analyze the PC kinetics. We rebuild them in the following scale: when turned on $[\ln(1 - (\sigma - \sigma_0)/(\sigma_{US} - \sigma_0)] = t/t_{on}$, and when switched off $\ln(\sigma - \sigma_0) = (- t/t_{off})$ (see Fig. 2c and d). Here, t_{on} and t_{off} are relaxation time constants of the LT stage when the ultrasound is switched on/off, respectively. First, we analyze the recovery curve (Fig. 2d), where the process goes without ultrasound. We see that the $\sigma(t)$ decrease passes along an exponential with characteristic time, $t_{off} \approx 32.4$ s. As for the LT of the $\sigma(t)$ growth stage when the US is turned on (Fig. 2c), taking the general temperature changes (Fig. 2a), we can assume that the process also has a thermoactivating part, and, similar to the PC growth stage, is not unique as both the AI $\sigma(t)$ growth occurs and there is a partial recovery in accordance with the process, $\ln(\sigma - \sigma_0) = (- t/t_{off})$ (see Fig. 2d). When saturation occurs, a dynamic equilibrium comes between the rate of return to the initial state and the rate of AI perturbation [$\sigma(t)$ growth]; the average time constant in this case is $t_{on} \approx 12.4$ s.

However, despite the formal similarity of AC with PC, we emphasize the fundamental difference between them. In the PC case, changes in $\sigma(t)$ are only related to carrier concentration, while, in the case of AC, there are changes of both concentration and mobility. In PC, quantum processes with electron redistribution between the levels (traps) and the conduction band are primary when the light is turned on, and only then certain diffusion long-term restructuring processes can occur in the point defect (PD) system caused by the change of the intracrystalline electric field.[3,11] In the case of AI processes, at the moment of ultrasound switching on, first the restructuring of PD complexes near oscillating dislocation segments occurs. These may be, in particular, AI transformations of DX centers into a metastable state at low temperatures.[15,16] In the process of AI dislocation oscillations, a new topography of local mechanical and electrical fields occurs, causing restructuring not only in the PD clusters but also in the dislocation structures.[17,18] The difference between the AC and the PC also reflects the distinct duration of the characteristic $\sigma(t)$ relaxation at growth and recovery. Indeed, when the ultrasound is switched on, the relaxation time is almost 2 times shorter than when it is switched off (Fig. 2). This experimental fact also confirms the diffusive nature of the AI local rearrangement of the point-defective crystal structure; as we know, the diffusion coefficient increases under US loading.[19,20] At the same time, the complete recovery of the relaxation curves at repeated ultrasound switching on at a fixed temperature shows the stability of the dislocation structure.

Temperature Characteristics for Separate Contribution of Individual Carrier Scattering Components

It is known that the mobility value is determined by different mechanisms of charge carrier scattering. The temperature dependences of the contribution of separate scattering mechanisms were estimated as follows. The scattering of neutral impurities, ionized impurities and dislocations have been considered. According to the Mattisen rule[21,22]:

$$1/\mu_{exp}^{0,US} = \Sigma(1/\mu_i^{0,US}) = 1/\mu_N^{0,US} + 1/\mu_{dis}^{0,US} + 1/\mu_{ii}^{0,US}, \quad (1)$$

were μ_{exp} is the experimental value, $\mu_i^{0,US}$ are the calculated mobility components when scattering on neutral impurities ($\mu_N^{0,US}$), dislocation scattering ($\mu_{dis}^{0,US}$), and scattering on ionized impurities ($\mu_{ii}^{0,US}$); and superscripts 0 and US correspond to the samples without and with ultrasound, respectively. The scattering by the lattice phonons is negligible for low temperatures where AI $\sigma(t)$ relaxation is observed.

The experimental temperature dependences of $\mu_{exp}(T)$ were fitted by Eq. 1 with help of the method of differential evolution,[12] and the contributions of different mechanism were estimated (see Fig. 1c). More details about the fitting procedure are given elsewhere,[9] but the main AI effects were the following:

1. the scattering on neutral impurities increases; the reason for the increase in neutral impurity concentration (from 4.6×10^{23} m^{-3} to 15.3×10^{23} m^{-3}) is the recharge (ionization) of certain centers and the decay of complexes;
2. the dislocation scattering, in our opinion thus deals with a decrease in the concentration of charged centers, located in the adjacent regions of the crystal;
3. the scattering on the ionized impurities weakens by reducing their effective concentration (from 5.5×10^{23} m^{-3} to 2.2×10^{23} m^{-3}).

Figure 6 shows the temperature dependences of AI relative changes in the mobility components:

$$\Delta_i(T) = (\Delta^{US}(\mu_i))/(\Delta^{US}(\mu_{exp})), \quad (2)$$

where

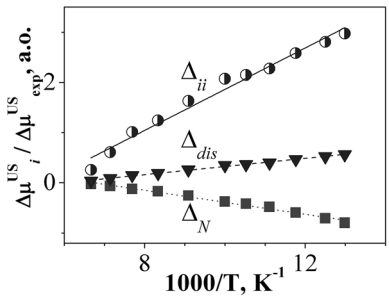

Fig. 6. Temperature dependences of AI relative changes of mobility components for various scattering mechanisms: on ionized impurities Δ_{ii}, on dislocations Δ_{dis}, and on neutral impurities Δ_N.

$$\Delta^{US}(\mu_{exp}) = 1/[(1/\mu^{US}_{exp}) - (1/\mu^{0}_{exp})];$$
$$\Delta^{US}(\mu_i) = 1/[(1/\mu^{US}_{i}) - (1/\mu^{0}_{i})]. \quad (3)$$

In Fig. 6, all three components change with the temperature decrease; however, the rates are different: $[\partial(\Delta^{US}_{ii}(\mu_{ii})/\partial T) = 0.31\ K^{-1}]$; $[\partial(\Delta^{US}_{dis}(\mu_{dis})/\partial T) = 0.08\ K^{-1}]$, and $[\partial(\Delta^{US}_{N}(\mu_N)/\partial T) = -\ 0.12\ K^{-1}]$. The highest temperature growth rate of the mobility component occurs on ionized impurities being 3–4 times higher than the rate of change of the dislocation scattering parts and that on the neutral impurities. The time ranges of the scattering mechanisms in $\sigma(t)$ relaxation is separated by comparing the value of $\partial(\Delta_i(T))/\partial T$ (Fig. 6) with the coefficients of the temperature changes of the ST and LT components (Fig. 3). For the dislocation and neutral impurity scattering parts characterized by small temperature change rates close to the ST part, we refer to the factors determining the ST of $\sigma(t)$. In our opinion, the dislocation scattering part can compensate for the negative character of the ultrasound influence on the neutral impurity components, especially because their temperature change rates are close to each other. The scattering on ionized impurities $\Delta_{ii}(T)$ changes the most with temperature, is responsible for the AI growth of $\sigma(t)$, and is attributed to the LT stage reason.

Features of Inhomogeneity Influence on AI Conductivity Changes

Consider another important factor influencing CdTe conductivity. The low values of mobility in samples at room temperature show a significant contribution to the scattering of charge carriers on crystal heterogeneity due to the accumulation of impurities in the CdTe:Cl.[23,24] How can this mechanism show itself under ultrasound? We have already suggested[8] that intensive US loading essentially weakens the inhomogeneity influence. The mechanism of such σ growth is the AI fluctuation decrease of the crystal potential relief. The $\Delta_N(T)$ dependence (Fig. 6) formally characterizes not only the AI change of neutral impurities concentration N_N but also the total electron scattering on the neutral impurity complex contribution change.

As for the kinetics of AI changes, it is worth emphasizing that such AI processes are athermic (the rate of state change coincides with the rate of external deformation change), i.e., changes in the inhomogeneity characteristics usually occurs through several periods of US loading. Therefore, we see the influence mainly in the ST stage. In fact, the weak temperature dependence of $\Delta_N(T)$ (Fig. 6) directly confirms this assumption.

Acoustical Dislocation Mechanism of Crystal Defect Structure Rebuilding

As already noted, the dislocations motion causes not only changes in the charge carriers scattering. Their main manifestation in the AI processes in A_2B_6 crystals is, in fact, the mechanical stresses of the acoustic wave localized in the scale of the crystal lattice and point defects determining the physical properties of a semiconductor crystal. One can see in Fig. 6 that the largest contribution of the AI changes in the CdTe:Cl crystal is the scattering decrease on the ionized impurities (μ_{ii}). Previous calculations make it clear that this thermoactivating mechanism causes the LT $\sigma(t)$ change.

Looking in more detail at the AI LT structural rearrangements near the dislocation clusters that, in general, determine the temporal nature of the LT, we note that, when the US is switched on for 10^{-6}–10^{-5} s, the sample volume oscillates with the US wave frequency; including PD clusters centered mainly around the dislocations. As a result of the forced dislocation oscillations (with an amplitude up to $\leq 10^{-8}$ m), the area of effective interaction of the dislocations with the electrons at traps enlarges; also, electrons are released from impurity levels.[8,9,17] One can assume that the concentration increase, Δn, with the atom oscillation amplitude in the US relates to an increase of the capture radius during the US process, i.e., an increase of the area swept by the dislocations.[9,17] In the course of the US, the distribution of the dislocation segments involved in AI oscillations can vary in length by thermoactivation (i.e., long-term), and there is a partial separation from weakly coupled centers of attachment. However, over time, the conditions of dislocations motion change somewhat. Even some reorganization of the dislocation structure is possible.[25]

This process can cause the capturing of many point defects (including charged ones, that reduces the ionized centers concentration N_{ii}) by dislocation traps, and then to the expansion of the region enriched by them.[26] As a result, the potential barrier reduces, and a non-stationary state of the PD structure occurs that seeks to adjust according to the new quasi-stationary electric-deformation conditions. These restructurings also involve some local acoustochemical reactions.[27]

We explain the increase of AI effects with temperature decrease by (1) a corresponding decrease of

phonon friction, whose magnitude mainly determines dislocations motion in semiconductor crystals, i.e., an increase of the velocity (and amplitude) of dislocations oscillation,[11,26] and (2) thermoactivation decreases and the population of metastable configurations increases.[15,16]

CONCLUSIONS

To find the mechanisms of relaxation of the acoustic conductivity $\sigma_{US}(t)$ in low-resistance n-CdTe crystals ($N_{Cl} \approx 10^{24}$ m^{-3}) in the temperature range 77–300 K, we investigated its kinetics with ultrasound switched on/off.

Separate comparison of the temperature dependences of the $\sigma_{US}(t)$ amplitude individual stages with the corresponding temperature changes in concentration and mobility allows us to associate acoustically induced concentration effects mainly with short-term (< 0.6 s) $\sigma_{US}(t)$ changes and AI effects of mobility changes mostly with long-term (> 100 s) ones.

Further analysis of the temperature characteristics for the separate mobility components contribution determined by certain mechanisms of carrier scattering make it possible to clarify their contributions to the ST or LT relaxation phases of $\sigma_{US}(t)$. Namely, we attribute the scattering mechanisms controlling the dislocation and neutral impurity components of mobility to the factors that mainly (along with concentration ones) control the short-term changes, and the scattering on ionized impurities to long-term ones.

It is suggested that possible mechanisms of acoustically induced conductivity changes are the transformation of the point defect complexes mainly in the near dislocation crystal regions and the consequent fluctuation decrease of the crystal potential relief.

ACKNOWLEDGMENTS

We express our gratitude to the employees of the Chernivtsi National University, M.I. Ilashchuk, A.A. Parfenyuk, and K.S. Ulyanytskyi, for supplying us with CdTe samples to investigate, and to Dr. W.H. Kozyrski at the Bogolubov Institute for Theoretical Physics for useful discussion.

REFERENCES

1. A.I. Vlasenko, Ya.M. Olikh, and R.K. Savkina, *Semiconductors* 33, 398 (1999). https://doi.org/10.1134/1.1187701.
2. V. Babentsov, S.I. Gorban, I.Ya. Gorodetskiy, N.E. Korsunskaya, I.M. Rarenko, and M.K. Sheinkman, *Sov. Phys. Semicond.* 25, 1243 (1991).
3. O.Ya. Olikh, *Superlattices Microstruct.* 117, 173 (2018). https://doi.org/10.1016/j.spmi.2018.03.027.
4. D.V. Korbutyak, S.W. Mel'nychuk, E.V. Korbut, and M.M. Borysyk, *Cadmium Telluride: Impurity-Defect States and Detector Properties* (Kyiv: Ivan Fedorov, 2000) (in Ukrainian).
5. I. Turkevych, R. Grill, J. Franc, E. Belas, P. Hoschl, and P. Moravec, *Semicond. Sci. Technol.* 17, 1064 (2002). https://doi.org/10.1088/0268-1242/17/10/305.
6. A.I. Vlasenko, Ya.M. Olikh, and R.K. Savkina, *Ukr. J. Fiz.* 44, 618 (1999).
7. Ya.M. Olikh and M.D. Tymochko, *Tech. Phys. Lett.* 37, 37 (2011). https://doi.org/10.1134/S106378501101007X.
8. Ya.M. Olikh and M.D. Tymochko, *Superlattices Microstruct.* 95, 78 (2016). https://doi.org/10.1016/j.spmi.2016.04.038.
9. Ya.M. Olikh, M.D. Tymochko, O.Ya. Olikh, and V.A. Shenderovsky, *J. Electron. Mater.* 47, 4370 (2018). https://doi.org/10.1007/s11664-018-6332-4.
10. M.I. Ilashchuk, A.A. Parfenyuk, and K.S. Ulyanitskyi, *Ukr. J. Fiz.* 31, 126 (1986).
11. I.P. Golyamina, eds., *Ultrasound. The Small Encyclopedia* (Moscow: Soviet Encyclopedia, 1979) (in Russian).
12. O.Ya. Olikh, *J. Appl. Phys.* 118, 024502 (2015).
13. M.K. Sheinkman and A.Ya. Shik, *Sov. Phys. Semicond.* 10, 209 (1976).
14. A.A. Ronassi and A.K. Fedotov. *Vestnik BGU*, Seriya 1. No. 2. 8 (2010).
15. B.N. Mukashev, KhA Abdullin, and YuV Gorelkinskii, *Phys. Usp.* 43, 139 (2000).
16. T. Thio, J.W. Bennett, D.J. Chadi, and R.A. Linke, Becla P (1996). *J. Cryst. Growth* 159, 345 (1996). https://doi.org/10.1016/0022-0248(95)00681-8.
17. YuA Osipyan, eds., *Electronic Properties of Dislocations in Semiconductors* (Moscow: Editorial URSS, 2000) (in Russian).
18. N.A. Tyapunina, G.V. Bushueva, G.M. Zinenkova, E.K. Naimi, and S.S. Novikov, *Crystallogr. Rep.* 55, 77 (2010). https://doi.org/10.1134/S106377451001013X.
19. V.N. Pavlovich, *Phys. Status Solidi B* 180, 97 (1993).
20. O.Ya Olikh and I.V. Ostrovsky, *Fiz. Tverd. Tela.* 44, 1198 (2002).
21. V.L. Bonch-Bruevich and S.G. Kalashnikov, *Semiconductor Physics* (Moscow: Nauka, 1977) (in Russian).
22. E.V. Kuchis, *Galvanomagnetic Effects and Investigation Methods* (Moscow: Radio i svjaz', 1990) (in Russian).
23. M.V. Alekseenko, E.N. Arkadyeva, and A.A. Matveev, *Sov. Phys. Semicond.* 4, 349 (1970).
24. B.I. Shklovskii and A.L. Efros, *Electronic Properties of Doped Semiconductors* (Berlin: Springer, 1984).
25. G.V. Bushueva, G.M. Zinenkova, N.A. Tyapunina, V.T. Degtyarev, AYu Losev, and F.A. Plotnikov, *Crystallogr. Rep.* 53, 474 (2008). https://doi.org/10.1134/S1063774508030152.
26. T. Suzuki, S.Takeuchi, and H. Yoshinaga, *Dislocation Dynamics and Plasticity* (Moscow: Mir, 1989) (in Russian).
27. V.L. Gromashevskyi, V.V. Dyakin, E.A. Sal'kov, S.M. Sklyarov, and N.S. Khilimova, *Ukr. J. Fiz.* 29, 550 (1984).